Developments in Diesel Spray Characterisation and Modelling

K. Karimi[1], E M. Sazhina[1], W. A. Abdelghaffar[1], C. Crua[1], T. Cowell[1], M R. Heikal[1], M R. Gold[2]

[1] School of Engineering, University of Brighton, Brighton UK

E-mail: E.M.Sazhina@brighton.ac.uk
Telephone: +44 (0)1273 642223
Fax: +44(0)1273 642301

[2] Ricardo Technical Centre, Bridge Works, Shoreham-by Sea, West Sussex, BN43 5FG

E-mail: Martin.Gold@ricardo.com
Telephone: + 44(0)1273 794036

Abstract. Experiments into the characteristics of Diesel fuel injection equipment (FIE) and fuel spray formation have been conducted on a high-pressure and temperature rapid compression machine (Proteus) to simulate realistic Diesel engine working conditions. Two multi-hole injectors, of the solenoid type, were used; one with a faster response actuator. A high speed video image acquisition system was used to characterise the liquid spray formation, penetration, cone angle, and general spray structure. The experimental spray penetration data have revealed the onset of spray tip instability (cluster shedding) at the later stages of spray penetration.

The instantaneous rate and shape of injection for different operating conditions has been measured using an injection rate-tube technique. The combination of the above techniques has allowed an alternative approach in the use of empirical spray penetration correlation to be modified in order to gain information on breakup length. This was achieved by way of the derivation of a breakup length proportionality constant, where historically, this constant was found experimentally.

An approach to the modelling of transient spray penetration based on the momentum conservation of the injected fuel mass as a physical body of varying mass under that action of the drag force acting on the whole body. For cases under consideration, this approach allows a better representation of early stage of spray penetration than the traditional modelling of each individual droplet under conventional Lagrangian approach which is widely employed by CFD codes. It is suggested that the method based on the Centre-of-Mass tracking can account better for the collective effects between droplets in a dense spray.

Nomenclature

A_n	*Nozzle (hole) exit area*
A	*Projected spray area corresponding to maximal width in lateral direction*
C_1	*Empirical constant*
C_d	*Discharge coefficient*
C_{Drop}	*Drag coefficient for a droplet*
C_D	*Drag coefficient for spray*
$C_{blasius}$	*Empirical constant for Blasius boundary layer thickness*
D_n	*Nozzle exit diameter*
L_b	*Breakup length*
L_{crit}	*Maximum penetration length at the onset of cluster shedding*
L_p	*Spray tip penetration length*
m_d	*Mass of a droplet*
$\dot{m}_f$	*Mass-flow-rate of fuel injection*
P	*Pressure*
$Re_{initial}$	*Reynolds number based on the injection velocity at the early stage of injection*
Re	*Reynolds number as defined in Blasius boundary layer model*
s	*Spray penetration based on distance travelled by the centre-of-mass of spray*
t	*Time from the start of injection*
t_b	*Breakup time.*
u_{inj}	*Injection velocity.*

u_{tip} *Spray tip velocity.*
u_d *Axial velocity of a droplet*
u *Axial velocity of the centre-of-mass for the injected fuel*

Greek Symbols

ρ_g *Ambient gas density*
ρ_l *Liquid fuel density*
ω *Breakup length's proportionality constant*
μ *Dynamic viscosity of air taken at TDC temperature*

Abbreviations

ICP *In-cylinder pressure*
TDC *Top dead centre*
VCO *Valve covered orifice*

1. Introduction

Emissions legislation is becoming evermore stringent. To ensure compliance, more effective and environmentally friendly combustion systems need to be designed and manufactured. There are several ways of meeting this challenge. Some engine designers favour exhaust gas after treatment, while other designers introduce more sophisticated fuel injection systems. In some cases, both technologies are applied side by side. However, the only way to reduce emissions at source is with the introduction of fuel injection systems capable of meeting the required demands for different engine load conditions. Different engine load conditions have a direct influence on the combustion process, which is dependent upon the quality and timing of the emerging fuel spray from the injector nozzle. The characteristics of the fuel spray are dependent upon many parameters such as injection pressure, in-cylinder pressure and temperature, nozzle size and geometry. Different combinations of these variables can provide the correct environment for a good combustion process. Although the influences of some of these variables are discussed in the literature, information on the effect of some of them is inconclusive. Some of these effects are presented in this paper, giving details of the experiments undertaken to characterise the fuel injection equipment (FIE) off the engine, and to define the emerging spray in a realistic engine environment for the above variables.

For the non visible part of the Diesel fuel spray such as the breakup length near the injector nozzle, information has been limited. The most widely known experiments (steady-state phase of injection) were conducted by Arai et al. (1984) and Chehroudi et al. (1985) with limited success. This is mainly the result of highly dense fuel spray in the vicinity of the nozzle exit. Due to these limitations, an indirect approach has been adopted for the prediction of the breakup length.

The breakup length is indicative of the fuel spray structure, but it is necessary to differentiate between the primary and secondary breakup modes. This is important from a modelling perspective regarding the application of an appropriate liquid jet or droplet breakup model. In the current study, the evolution of the breakup length has been examined during the steady-state and initial phases of injection. Analysis of the breakup length during the initial spray phase characterises the transition from the start of injection to the near-constant value apparent during the steady-state phase. With ever-decreasing injection durations (with reference to multiple injection strategies, and increased number of holes) the spray transient behaviour during this initial phase becomes predominant, as it accounts for a larger proportion of the overall injection duration.

For the characterisation of the FIE, the long-tube rate of injection technique was applied. This technique allowed instantaneous measurements of rate of injection, and hence, the injection velocity and the discharge coefficient to be analysed. High-speed visualisation was applied for the characterisation of Diesel fuel spray parameters such as penetration rate, spray cone angle, and spray breakup (Crua, 2002, Hattori et al., 2002, Heimgartner and Leipertz, 2000, Karimi, 1989, Kennaird et al., 2002).

2. Experimental Set-Up

2.1 The Long-Tube Rate of Injection Technique and Set-up

The Long-Tube method is the standard technique to measure the rate of injection. It has been developed in parallel with the fuel injection equipment (FIE) of Diesel the diesel combustion engine over many years. A comprehensive study and comparison of various rate measurement techniques are presented by Baniasad (1994). Only the basic operating concept of the Long-tube rate gauge method is described here: the fuel is injected into a long tube (delay line) containing the same working fluid under pressure, this in turn creates a pressure wave which travels along the tube at the speed of sound in the fluid. The theory of pressure waves in liquids states that, at any instant in time, the magnitude of the pressure wave is directly proportional to the flow velocity at a given cross section in the tube. Given a tube of uniform cross sectional area, the flow velocity, and hence pressure, is proportional to the rate of injection (Lucas, 1995).

Fitted to the gauge near the injector nozzle outlet (in the rate meter), a pair of strain gauges measure variation in the pressure waves, and a second pair are used for temperature compensation (Fig 1). The strain gauges were connected to a bridge amplifier and the output was displayed on a storage oscilloscope. The rail pressure, injector current, and the Transistor Transistor Logic (TTL) signals were also recorded on the storage scope for analysis. The variation in rail pressure, the delay in commencement of injection and the time response for needle full lift were also recorded. For all traces, an average of 100 cycles was recorded and compared with instantaneous recordings to ensure repeatability.

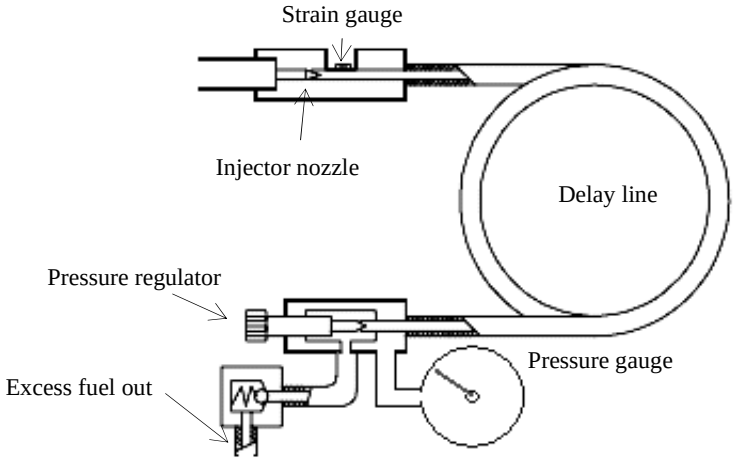

Fig. 1. Schematic diagram of Lucas rate tube

The required pressure within the delay line was adjusted with a pressure valve regulator. This allowed simulation of in-cylinder pressure at the time of injection.

2.2 Proteus Spray Rig

The Proteus is a single cylinder two-stroke rapid compression machine, with a specially designed head for optical access for spray visualisation (Fig 2). As a result of the spray chamber cavity forming the top of the combustion chamber the compression ratio is only 9:1. Therefore in order to develop in-cylinder pressures and temperatures representative of a modern Diesel engine, the boost pressure and intake air temperature were increased, giving nominal TDC pressures of up to 12 MPa, and a TDC motored gas temperature of 785 K (for a comprehensive description of the Proteus rig, see Kennaird et al., 2000 and Crua, 2002.

The optical head of the Proteus engine was designed to result in near quiescent air conditions in the spray chamber with a maximum predicted local air velocity of 1 ms^{-1} in order to avoid disturbance of the spray development by the air motion, as well as to achieve maximum loop scavenging efficiency in the combustion chamber. In addition, this design has the added advantage of allowing study of the air entrainment created by the emerging liquid spray itself. The spray chamber within the optical head was cylindrical, and had dimensions of 25 mm in radius, and 80 mm in height. This allowed sufficient space for the spray to develop without any wall impingement.

Two Kistler pressure transducers were fitted to the engine combustion chamber. The first was a water cooled Kistler 6061 fitted to the optical head to monitor the in-cylinder gauge pressure with a range of 0-20 MPa. The second pressure transducer was a Kistler 4045-A10 with a range of 0-1 MPa fitted just above one of the inlet ports in the combustion chamber to monitor the absolute boost pressure. The Proteus engine was coupled to a DC dynamometer via reduction belts (6:1). With an operating speed of 3,000 rpm at the dynamometer, a corresponding engine operating speed of 500 rpm at the flywheel was reached.

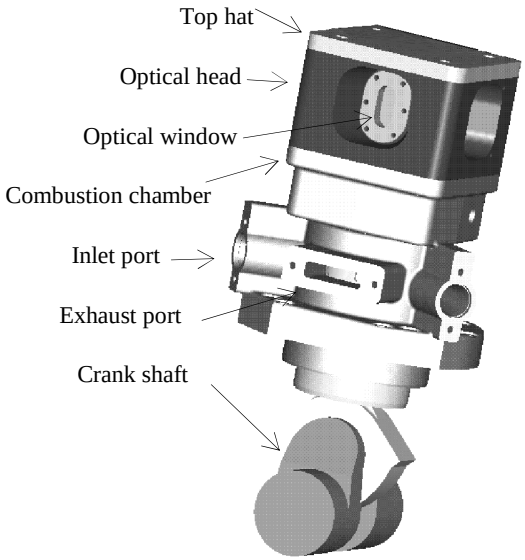

Fig. 2. CAD drawing of the Proteus Engine

A second generation common rail fuel injection system was used to generate the injection pressures ranging from 60 to 160 MPa. The fuel pump was driven externally by an electrical motor running at 1,400 rpm to maintain the required high pressure in the fuel rail with minimum fluctuation. The two injectors used throughout the current experiment were a 3 hole 0.2 mm diameter valve covered orifice (VCO), and a 7 hole 0.135 mm diameter VCO injector. Each injector in turn was mounted in one of the four openings arranged around the optical head forming the spray chamber; the other three openings contained the windows.

2.3 High-Speed Image Acquisition System and Set-up

A Phantom V7.1 high-speed camera was used for spray visualisation. The camera featured an 8-bit monochromatic CMOS sensor, and a global electronic shutter with speed up to 2 μs. The recording rate is adjustable up to 4,800 frames per second at full resolution (800 × 600), and 4,800 to 150,000 frames per second at progressively reduced resolution. Compromise between acquisition rate and resolution was obtained with a frame rate of 34,300 frames per second, with a corresponding maximum resolution of 128 × 320. In order to maximise the intensity of the recorded images, the gamma correction factor was set to 1.0. To ensure the best possible image recording, a black reference level (background grey level reference) was performed prior to capturing and recording of the images. This black reference was set automatically by the camera at a level of 40 (out of 256 levels of grey for an 8-bit camera). Two 125 W halogen flood lights fitted with diffusers were used as shown in Fig 3, each one focused on the fuel spray axis from opposite sides.

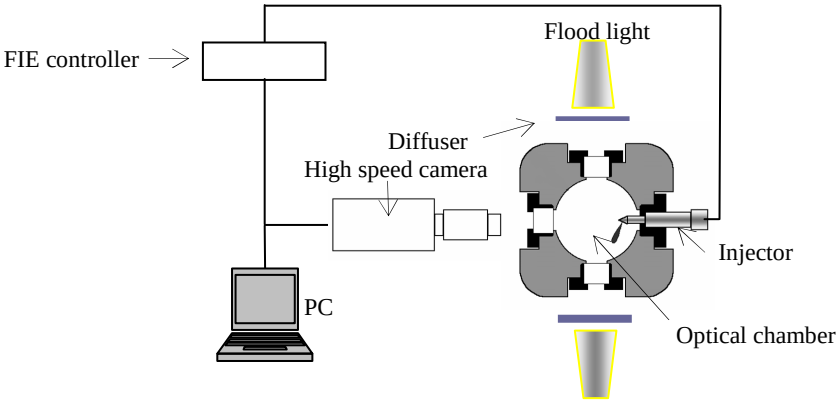

Fig. 3. Schematic diagram of the experimental set-up for side-lit spray photography

This set-up gave the best homogeneous illumination of the spray background (as opposed to backlighting). The processing of the video images for measurement of the spray penetration was performed by purpose-developed software (Crua, 2002). Suitable pixel thresholding was carried out in order to pick out the tip of unbroken portion of the spray outline, furthest from the nozzle on the spray axis (± 1 pixel) from the background.

3. Results

3.1 Off-Engine Injector Characterisation

With the Long-tube rate gauge calibrated, the back pressure within the delay line was set to 2, 4 and 6 MPa respectively, corresponding to in-cylinder pressures of the same magnitude at TDC. Injection commenced with injection pressures set between 60 and 160 MPa. From the experimental data on the rate of injection ($\dot{m}$) the instantaneous injection velocity (u_{inj}) as well as the evolution of discharge coefficient (C_d) with respect to time were derived using continuity and the equation defining discharge coefficient - Eq.(1)

$$u_{inj} = \frac{\dot{m}_f}{\rho_l A_n},$$
$$C_d = u_{inj}\sqrt{\frac{\rho_l}{2\Delta p}}, \qquad (1)$$

where ρ_l is the density of the injected fuel, A_n is the area of one nozzle hole outlet, and ΔP is the instantaneous pressure difference between the injection pressure and in-cylinder/back pressure. A_n should be multiplied by the number of nozzle holes for a given injector. It should be noted that in this study the equivalence diameter is considered constant, and thus the nozzle contraction area is neglected. This hypothesis is considered acceptable since the contraction will be minimal during the initial phase of the injection.

Results presented in Fig 4 demonstrate the evolution of C_d as the injector needle lifts. The increase from zero to a relatively steady value occurs at about 0.5 ms after commencement of injection. This period is consistent with the recorded needle lift traces. Other researchers had previously assumed that the transient evolution of C_d occurred over a period less than 0.1 ms (Yule and Filipovic, 1991). With the introduction of shorter injection durations, it is increasingly important to take into account the transient value of C_d.

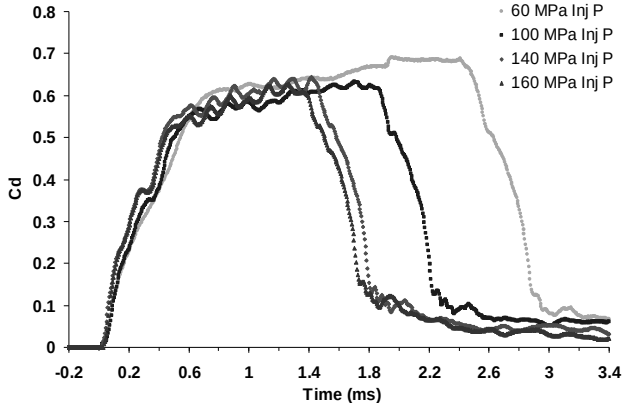

Fig. 4. C_d as a function of time, for a 0.2 mm single guided 3 hole VCO nozzle at 4 MPa back pressure, and 50 mm^3 fuelling

3.2 Spray Characterisation

The spray structure of Diesel fuel was observed with the high-speed Phantom video camera as explained in section 2.3. The data was gathered for three different in-cylinder pressures (ICP) at top dead centre (TDC) (2, 4, and 6 MPa), and four different injection pressures (60, 100, 140, and 160 MPa) at two different air intake temperatures 'cold' (293 K) and 'hot' (373 K), resulting in TDC temperatures of 570 K and 720 K, respectively. Each test was repeated three times in order to ascertain repeatability for liquid spray penetration and spray cone angle. On the basis of the images obtained, there exists a high density portion (intact liquid core) where the spatial distribution of the liquid fuel is uniform relatively close to the nozzle tip. Further downstream of the nozzle tip, the high density portion begins to breakup, and a surface wave is generated on the outer edge of the spray structure. Fig 5 (a) and 5 (b) show the results of tests at in-cylinder pressures of 2 and 6 MPa respectively. Each contains a series of test images for increasing injection pressures at 0.41 ms after first sight of fuel and at an ambient temperature of 576 K at TDC.

As expected, penetration length increased with increasing injection pressure and decreased with increase in ambient gas density. These observations are consistent with previous studies by Arai et al. (1984), Hiroyasu and Arai (1990), Kennaird et al. (2002), Naber and Siebers (1996), and Reitz and Diwakar (1987).

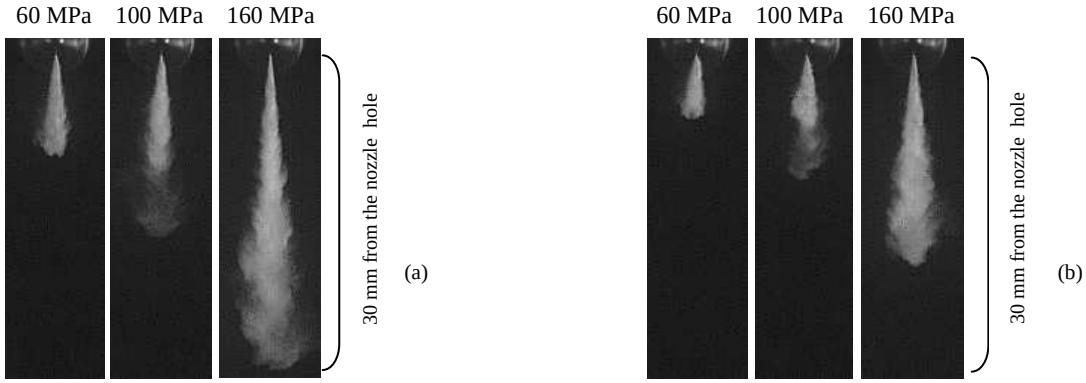

Fig. 5. Spray images taken at in-cylinder pressures of 2 MPa (a) and 6 MPa (b); 0.41 ms after first sight of fuel

The above images also show that the interaction between the stagnant gas field and the leading edge of the spray during the initial stages of injection has the effect of compressing clusters of droplets together as the spray jet penetrates. Further downstream of the nozzle, the exchange of momentum between the droplets and the local gas field allows entrainment of dense air along the edges of the spray. The effect of this is smaller clusters of droplets stripping back or detaching from the bulk of the spray. At the leading edge however, when the spray is fully developed, larger clusters of droplets are starting to detach as the air entrainment increases at the same time as the droplet momentum decreases (Fig 6).

The level of stripping and detachment of droplets was observed to be dependent on the magnitude of injection and in-cylinder pressures. They are the result of increased liquid surface area at higher injection pressures,

and increased gas density at high in-cylinder pressures. For higher in-cylinder pressures, this can also be viewed as the result of higher tangential stresses acting on the moving spray which leads to stripping and detachment of clusters of droplets as well as individual droplets breaking up.

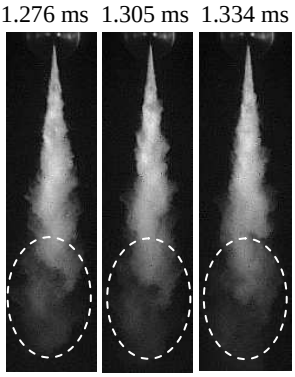

Fig. 6. High-speed video sequence in steps of 29 μs showing droplet clusters starting to detach along the leading edge of the spray at cold intake

For the range of injection pressures tested, no significant variation of the spray cone angle was observed (for the steady state period of injection). Typically, the full cone angle was measured as 18º for the 3-hole 0.2 mm VCO nozzle, and 12º for the 0.135 mm diameter VCO single guided 7-hole nozzle.

3.3 Modelling of Spray Penetration Length from First Principles

The task of predicting spray penetration is often delegated to a multidimensional CFD simulation of the spray for high accuracy. Traditionally, such modelling is performed either under the Eulerian approach for both liquid and gas phases, or under the Lagrangian (for liquid) – Eulerian (for gas phase) approach. The Lagrangian-Eulerian approach is a popular tool for engineering applications such as spray formation in an internal combustion engine. Under this approach, the spray is modelled as an ensemble of droplet parcels. Each parcel is injected with a specified injection velocity (or mass flow-rate) at a certain time within the injection duration, and is characterised by its own droplet size and temperature. The equations of motion for each droplet parcel are solved alongside the Navier-Stokes momentum conservation equations for the gas phase. It is not uncommon however to find that in some cases the results of such sophisticated simulation do not show a good agreement with the experimental spray penetration data. Moreover, the predictions sometimes can be worse than those from a simple one-dimensional spray model, or from an empirical correlation. Therefore, the current work investigates possible reasons for such discrepancies, by means of a parametric study under realistic engine conditions for cold air intake in the Proteus rig.

Under the traditional Lagrangian approach, the equation of motion of a droplet of a mass m_d in the direction of spray axis, reads:

$$\frac{d(m_d u_d)}{dt} = -\frac{1}{2} C_{Drop}\ \rho_g\ A_d\ (u_d - u_{gas})^2, \qquad (2)$$

where u_d and u_{gas} are droplet and gas axial velocities respectively, and the drag coefficient for an isolated droplet C_{Drop} is a function of Reynolds number (Sazhin et al., 2003, and others). This equation is solved in a coupled way with the equations of droplet motion in the other two dimensions, and the equations for droplet temperature and mass. Following Sazhin *et al.* (2003) it is assumed that there is no significant heat and mass transfer between droplets and in-cylinder gas under cold intake conditions. The radial and circumferential components of the injection velocity were assumed to be zero since there was no swirl in the injector, and the in-cylinder gas was quiescent.

In a framework of a CFD code, a droplet exchanges momentum with the gas phase while it is assumed that it does not experience any drag force due to the interaction with other droplets. This underlying assumption for modelling of isolated droplets is well suited for a dispersed spray. A well-known limitation of this modelling approach is that the volume fraction of liquid should be much less than the volume fraction of gas phase. In what follows we will examine the validity of this approach for our experimental cases.

A popular approach is based on droplet tracking governed by Eq. (2) with an average value of injection velocity estimated from the difference between injection and in-cylinder pressures (as in Eq.(1)). The effective value of constant discharge coefficient (*Cd*) is often adjusted in order to give a good agreement with the experimental data. This approach satisfactorily describes many experimental cases although in some cases it cannot represent the overall shape of the spray penetration curve (Sazhin et al., 2003). In our case, the initial stages of spray penetration data as obtained from high-speed video images, were underpredicted by Eq. (2) for all realistic values of discharge coefficient, and drag coefficient for the droplets(Prof A. Shraiber, Private Communication).

It could be argued that this is due to the assumption that the injection velocity is constant and taken at some average level not representing the peaks. Hence it is believed that a multidimensional CFD simulation employing a realistic injection profile and tracking many thousand of droplets should remedy the problem. Below we show an asymptotic study of the validity of this assumption by a one-dimensional code imitating the workings of the relevant part of a CFD code.

A typical transient injection velocity profile, as obtained from the long-tube rate experiment, is shown by the red curve in Fig 7, whilst the black curve shows the spray tip velocity derived by numerically differentiating the spray tip penetration L_p. Under the simulation by the code, a droplet is injected each 5 microseconds (the same resolution as the long-tube experiment) with the velocity corresponding to the instantaneous injection velocity at this moment of time. Hence a droplet injected at about 0.075ms is much faster than that injected at 0.025ms, and it can overrun the earlier injected droplets after some time. Thus the tip penetration can be expected to be associated with the fastest droplets in the ensemble rather than the droplets injected earlier with some average velocity. Hence reproducing the peaks of the injection profile could allow a better agreement with the experiment under conventional Lagrangian droplet tracking. This approach is employed by multidimensional CFD codes; the number of parcels can be very large, a typical simulation can easily exceed 10,000 droplet parcels (Sazhina et al,, 2000). Such a fine resolution can reproduce experimental data quite closely in many cases, while persistent underprediction of spray penetration is still observed in some cases.

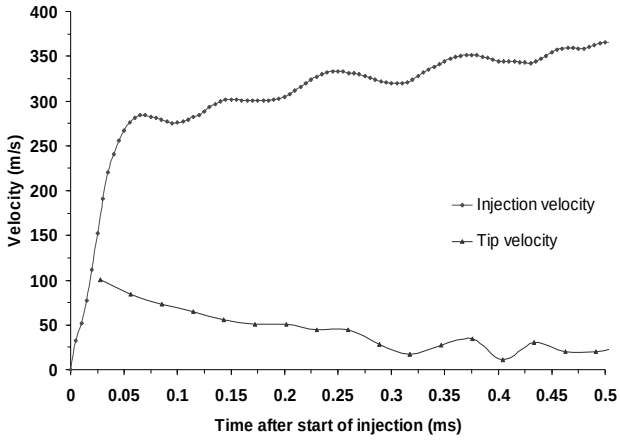

Fig.7 Evolution of injection velocity obtained from the rate measurements, and the tip velocity obtained by differentiation of the penetration data; injection pressure 140 MPa; in-cylinder pressure 6 MPa cold air intake; 0.135 mm VCO single guided 7 hole nozzle

For the case shown in Fig 7, an underprediction of penetration at the initial stages was obtained by the in-house 1-D FORTRAN code based on Eq. (2) with the drag coefficient expression taken from Sazhin *et al.* (2003) and the injection velocities profile from the long-tube experiment. Hence a parametric study was carried out to establish the upper limit of the calculated spray penetration. Setting the drag force to zero should give the maximum possible penetration under the approach based on Eq. (2). The correct injection velocity at each time step was used as the input for the initial velocity of each droplet in the ensemble. The droplets were launched every 0.005ms with the same resolution as the long-rate tube experiment. The results of the calculations against spray tip penetration are shown in Fig 8.

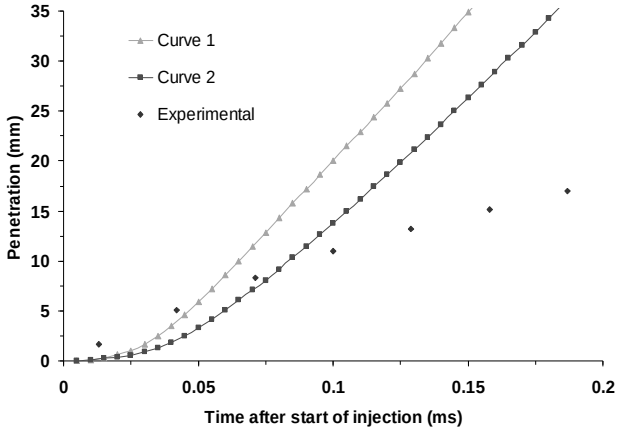

Fig 8. Comparison between experimental and calculated spray tip penetration. Calculations are performed under assumption of spray as a rigid body moving out axially with the velocity equal to the instantaneous injection velocity (curve 1). Curve 2 shows spray penetration calculated as the maximal distance travelled by an ensemble of droplets under Lagrangian tracking. The droplets are injected at a certain time after start of injection with the appropriate injection velocity. The absence of drag on the droplets establishes the upper limit for spray penetration.
Experimental spray tip penetration is for 140 MPa injection pressure; 6 MPa in-cylinder pressure, cold air intake; injector with VCO single guided 7-hole nozzle, 0.135 mm hole diameter

The spray tip trajectory (curve 2 in Fig 8) is the result of superposition of individual droplet trajectories. Each droplet trajectory is a straight line with the slope defined by the value of injection velocity at the moment of droplet injection. As it can be seen from the figure, even in this asymptotic case of the absence of drag force, the code based on Eq. (2) still gives underprediction of penetration at the initial stage. This demonstrates that under current modelling approach based on Eq. (2), the experimental data on spray penetration at the initial stages cannot be reproduced. Moreover, the shape and slope of the calculated spray penetration is very different to the experimental one.

The deficiency of the model for this case can be associated with ignoring the group effects between droplets. While Equation (2) is well suited to the droplet tracking of isolated droplets interacting with the gas phase via the drag force, the drag force due to the interaction with other droplets is not accounted for.

Under another popular modelling approach, a spray penetration curve is based on the concept of a spray as a rigid body. In other words, the spray penetration is given by the area under the injection velocity curve in Fig 7. It does not reproduce well the slope of the experimental curve either, as can be seen from Fig 8.

Hence a modelling approach for a dense spray as a physical body was sought from first principles. This approach is based on the conservation of momentum as in Eq. (2), but it is applied to the whole spray. This approach follows ideas of Sazhin et al. (2001), but here it is extended to the transient injection velocity experimental profile as an input into the calculations. The equation for mass and momentum conservation for the spray can be written as:

$$\frac{d(mu)}{dt} = \rho_l \; A_n \; u_{inj}^2 \; - \frac{1}{2} C_D \; \rho_g \; A \, u_{tip}^2 \; , \qquad (3)$$

where C_D is the drag coefficient for the whole spray (as opposed to a droplet), A is the projected spray area, u_{tip} is the tip velocity of the spray, and u is the velocity of centre of mass of the spray. In Eq. (3), m is the mass of injected liquid fuel at a given moment of time, $m = \int_0^t \dot{m}_f \, dt$ where mass-flow-rate $\dot{m}_f = \frac{dm_{inj}}{dt}$ is measured experimentally, and t is the time from start of injection.

It should be observed that the tip velocity u_{tip} should be close to the velocity of the centre-of-mass u of a continuous spray, in the absence of major spray instability such as cluster shedding. This is a reasonable assumption for a parametric study of the drag force acting on the injected fuel mass as a physical body. Hence we can rewrite Eq. (3) as:

$$\frac{d(mu)}{dt} = \rho_l \, A_n \, u_{inj}^2 \, - \frac{1}{2} C_D \, \rho_g \, A \, u^2 \qquad (4)$$

The drag coefficient C_D for the spray as a bluff deformable body in the presence of air entrainment and droplet stripping is quite difficult to evaluate. For our parametric study we will follow the approach developed by Mulholland et al. (1988). They explored drag coefficient in an ensemble of droplets as a function of droplet spacing.

For a very dense spray (when the spacing between droplets tends to zero) they used the expression for drag on a rod given as $C_D = 0.7555/Re_{initial}$ where the Reynolds number, $Re_{initial}$ is based on the value of the rod diameter and its velocity. We will employ this expression for drag coefficient for a spray immediately after first sighting of fuel out of the nozzle. The value of Reynolds number at the early stage of injection $Re_{initial}$ will be defined by the nozzle diameter and some initial value of injection velocity. The latter can be considered a tuneable parameter of the model since the injection velocity in Fig. 7 varies with time, growing from zero at the initial stage of spray penetration.

The maximum value of the drag coefficient for the spray is assumed to be equal to $C_D = 1.54$. This value is given by Liu and Reitz, (1993) for a deformable droplet. It is assumed that for the spray, it is reached at the onset of cluster shedding when the maximum unbroken length of the spray from the nozzle L_{crit} is reached. A linear variation of the drag coefficient is assumed between these two conditions under our parametric study. Thus, the expression for the drag coefficient as a function of penetration length becomes: $s \le L_{crit}$

$$C_D = \frac{0.755}{\mathrm{Re}_{initial}} + \left(1.54 - \frac{0.755}{\mathrm{Re}_{initial}}\right)\left(\frac{s}{L_{crit}}\right), \qquad (5)$$

where L_{crit} is the maximum penetration length at the onset of cluster shedding as shown in Fig 9, and $\boldsymbol{s}$ is the position of centre-of-mass of the spray, $s = \int_0^t u dt$

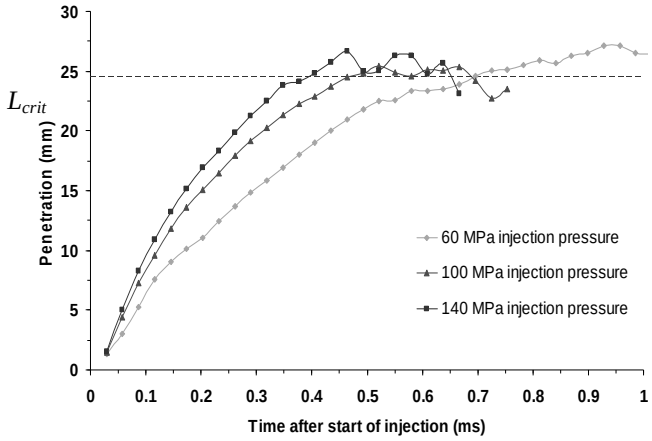

Fig. 9. Effect of injection pressure on spray penetration for a 0.135 mm 7-hole single guided VCO nozzle, at 6 MPa in-cylinder pressure and cold air intake, showing the definition of L_{crit}

The drag force is augmented by air entrainment and therefore the projected spray area $\boldsymbol{A}$ in (4) should account both for the liquid part of the spray, and the boundary layer around it. The former contribution is the area of a circle with radius equal to the sum of nozzle radius and the product of $\boldsymbol{s}$ and the tangent of half the cone angle. The latter is taken in the Blasius form (Douglas, 1995) as a thickness of boundary layer over a plate. Hence

$$A = \pi\left(0.5D_n + s\tan\frac{\theta}{2} + C_{blasius}\frac{s}{\sqrt{\mathrm{Re}}}\right)^2, \qquad (6)$$

where $C_{blasius}$ is the scaling constant, D_n is the nozzle diameter and *Re* is the Reynolds number under the Blasius definition $\mathrm{Re} = \frac{\rho_g s u}{\mu}$. For the given injector, the value of the cone angle is $\theta = 12°$.

The integration of Eqn (4) gives the position of the centre-of-mass of the injected liquid fuel (**s**), and therefore it is expected that the calculated values of *s* should not exceed the experimental values of spray tip penetration L_p. The value of *s* can be identified with the position of the centre-of-mass of the spray in the absence of evaporation (cold intake in our case) and air entrainment. Sensitivity studies for air entrainment did not show any significant influence on the results even when the mass of entrained air was taken as high as 10% of the injected fuel mass.

It should be clearly indicated at this stage that our aim is to track the position of the centre-of-mass of the liquid fuel (with a view that it could be employed for an improvement of CFD Lagrangian modelling) rather than to simulate the exact position of the spray tip (which is subject to the choice of the threshold level for the spray images).

Under our parametric study we compare the trends in the penetration curves until a major spray instability such as cluster shedding occurs. As it can be seen from Fig 10, this approach gives a reasonable agreement with the experimental penetration data.

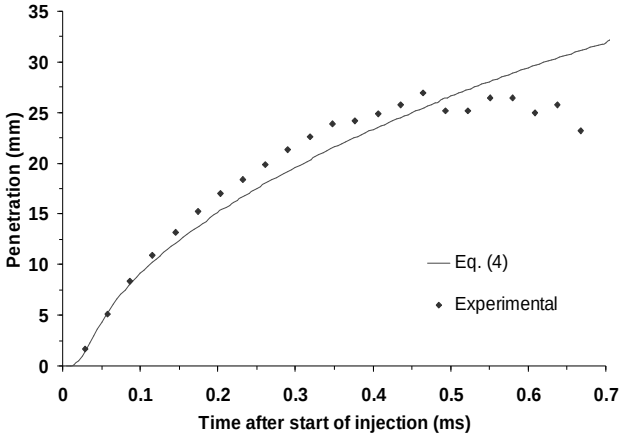

Fig.10 Calculated position of centre-of-mass for the injected fuel and experimentally observed spray tip penetration for a 0.135 mm diameter 7-hole single guided VCO nozzle, at 140 MPa injection pressure and 6 MPa in-cylinder pressure at TDC; cold intake. The model parameters are $Re_{initial} = 0.831$, $C_{blasius} = 50$. Experimental value of cluster-shedding length $L_{crit} = 24.5mm$ can be assessed from the in Fig 9

For validation purposes, the method was applied to the same injector but for in-cylinder pressure of 2MPa. The results can be seen from Fig 11.

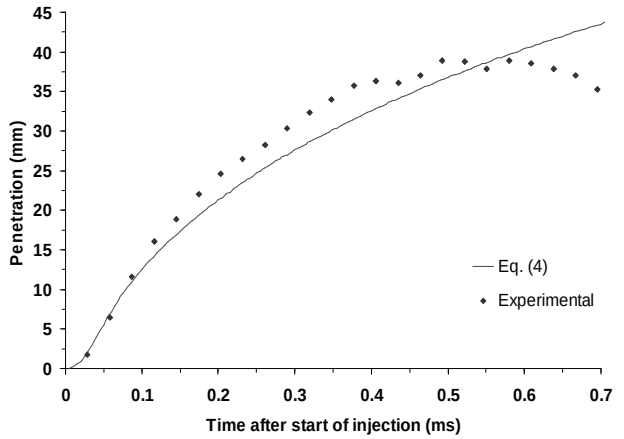

Fig.11 Calculated position of centre-of-mass for the injected fuel and experimentally observed spray tip for a 0.135 mm 7-hole single guided VCO nozzle, at 140 MPa injection pressure and 2 MPa in-cylinder pressure at TDC; cold intake. The model parameters are $Re_{initial} = 0.831$, $C_{blasius} = 1$. Experimental value for $L_{crit} = 37.5mm$

The experimental data presented in Fig 11 show a reasonable agreement when compared with the calculated results for the same value of $Re_{initial}$ but for a lower value of $C_{blasius}$. A larger thickness of the boundary layer in the former case is attributed to enhanced stripping of droplets by air of higher density. This is in agreement with experimental observations of Section 3.2.

To summarise, for the cases under consideration, the conventional droplet tracking algorithm based on Eq. (2), underpredicts spray penetration at the initial stage, even in the absence of the drag force. On the other hand, the model based on Eq. (4) for the conservation of mass and momentum for the whole injected liquid fuel mass, is able to reproduce the overall shape of experimental curve until the onset of cluster shedding. In particular, it is able to predict the curve shape for the initial stage of spray penetration.

It should be noted that the results were rather insensitive when taking into account increase of spray mass due to air entrainment. Droplet evaporation was neglected under the conditions of cold intake. Both these conditions can be generalised in a straightforward way to include evaporating droplets and air entrainment into the spray.

It is suggested that ignoring the group effects between droplets is not justified for a dense spray. This assumption works well in dispersed sprays when volume fraction of liquid is much lower than that of gas phase. For initial stage of a dense spray penetration, the interaction between fluid elements in the spray cannot be neglected.

This opens a possibility of improving the conventional CFD algorithm for dense sprays. As a suggestion for future work, this may be achieved by taking into account that the drag force is produced both by the interaction with the rest of the spray droplets, and a contribution from in-cylinder gas.

Such an approximation for a droplet in dense spray could hold until the distance travelled by the droplet is less than the empirical breakup length which will be defined in the next section.

3.4 Empirical Modelling of Breakup Length and Breakup Time Based on Penetration Correlation

The prediction of global parameters of spray, such as the breakup length and breakup time, has great practical importance. One way to predict such phenomena is based on empirical correlations.

The penetration profile data gathered in the current test were compared to the general penetration correlation of the form used by Dent (1971); Hiroyasu and Arai (1990), described in the following equation:

$$L_p = C_1 \left(\frac{\Delta P}{\rho_g} \right)^{1/4} (D_n t)^{1/2} \tag{7}$$

Where L_p is the spray penetration length, C_1 is an empirical constant, ρ_g the ambient gas density, D_n the orifice diameter, and t is the time after start of injection.

The value of C_1 can be considered as the product of the integration constant, the discharge coefficient (C_d), and the proportionality constant (ω) for the breakup length (Dent, 1971). Therefore C_1 can be written as:

$$C_1 = \left(\sqrt{2\sqrt{2}} \right) (\omega . C_d)^{1/2}, \tag{8}$$

and where the break-up length proportionality constant (Arai et al, 1984, Chehroudi et al., 1985) is defined by:

$$L_b = \omega D_n \sqrt{\frac{\rho_l}{\rho_g}} \tag{9}$$

Least squares fit of Eq. (7) against the experimental data over a range of injection pressures (60 to 160 MPa) and in-cylinder pressures (2 to 6 MPa) gave a consistent value of 2.15 for the empirical constant C_1. See Fig 12.

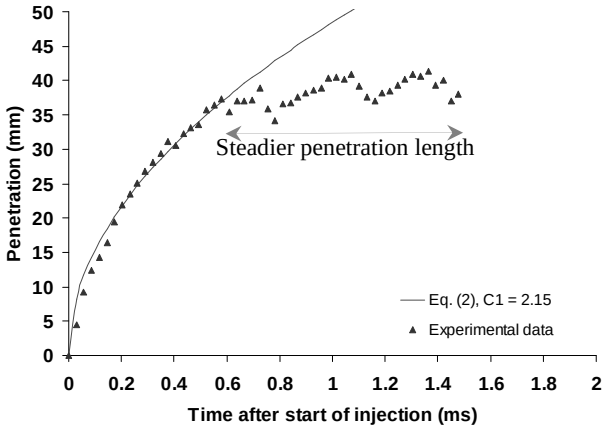

Fig. 12. Comparison between empirical constants and experimental data; the experimental results are for non-evaporating spray (cold intake); 160 MPa injection pressure; 4 MPa ICP**,** 24.2 kg m^{-3} ambient gas density

By substituting the new value of the empirical constant (C_1 = 2.15) into Eq. (8), and substituting for ω in Eq. (9) gives:

$$L_b = \left(\frac{\left[2.15 / \left(\sqrt{2\sqrt{2}} \right) \right]^2}{C_d} \right) \left(D_n . \sqrt{\frac{\rho_l}{\rho_g}} \right), \qquad (10)$$

where $D_n (\rho_l / \rho_g)^{1/2}$ is the equivalent hole diameter (Yule and Filipovic, 1991) through which the same mass flow rate of nozzle fluid would emerge, as well as having the same momentum, but with a density ρ_g instead of ρ_l (Thring and Newby, 1952; Dent, 1971). Since the nozzle contraction was neglected, the values of L_b calculated using Eq. (10) will be maxima.

During the initial stage of injection the core remains intact and there is no break-up. At some point the penetration and the liquid core lengths diverge due to the surface waves acting on the edge of the spray and the break-up length is reached. Hence, using Eq. (10) and the transient C_d data it is possible to derive the subsequent evolution of the breakup length with time, for the remainder of the injection phase. Fig 13 illustrates the breakup length as a function of time for a range of in-cylinder pressures. Since the C_d values rise rapidly from zero at time zero, the effective break-up length from Eq. (10) would initially be predicted as infinitely large. To identify the point of real initial break-up, the point is identified at which the predicted break-up curve crosses the penetration curve.

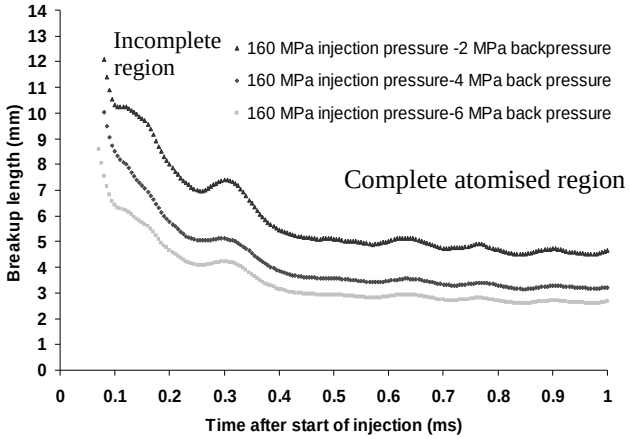

Fig. 13. Maximum breakup length (L_b) as a function of time from start of injection, and 50 mm^3 fuelling

As can be seen from Fig 13, the breakup length shows a significant reduction as the in-cylinder pressure increases. This increase is evident during the complete and incomplete atomised region.

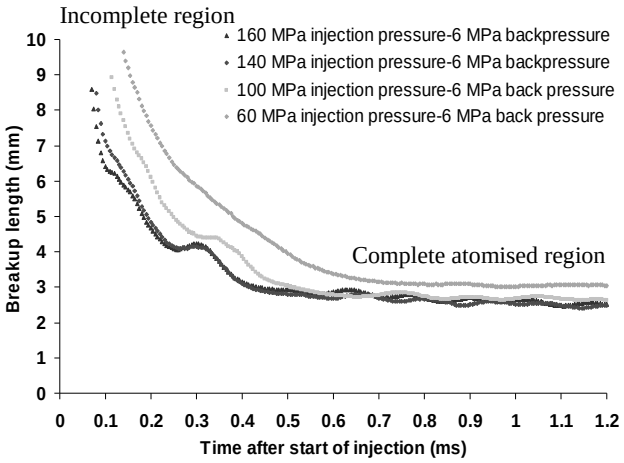

Fig. 14. Maximum breakup length (L_b) as a function of time from start of injection, and 50 mm^3 fuelling

However, Fig 14 shows that the reduction in the breakup length during the early stages of injection (in the incomplete region) is more rapid as the injection pressure increases, than in the complete atomised region. The increase in injection pressure, contributes to the needle opening velocity, and thus, more rapid uncovering of the nozzle hole as the pressure increases. Once the needle has reached its maximum lift position, the discharge coefficient (C_d) becomes steady if needle oscillations are neglected. Any further increase in injection pressure at this point, results in no substantial decrease of the breakup length for the range of pressures carried out in this study.

Conclusions

- The general penetration correlation with a new empirical constant gave a good fit to the experimental data. This also allowed an indirect determination of the initial and developing breakup lengths, applicable for complete and incomplete atomisation regions (transient spray). This technique can be applied to any fuel injector.
- The reduction in breakup length during the complete and incomplete region is the result of increased in-cylinder gas density and the injection pressure assuming a constant effective nozzle diameter. No significant change in length due to an increase in injection pressure in the complete atomised region was observed for the range of injection pressures tested. However, if one assumes a reduction in the actual flow area within the nozzle, a further reduction of the breakup length within the complete atomised region is clear.
- For the cases under consideration, the conventional droplet tracking algorithm as used in CFD codes, under predicts spray penetration at the initial stage, even in the absence of drag force.
- The model based on the conservation of mass and momentum for the whole spray as a physical body is shown to produce a reasonable agreement between the numerical and the experimental results. This opens a possibility of improving the conventional CFD algorithm for dense sprays.

Acknowledgment

The authors are grateful to the European Regional Development Fund Franco-British INTERREG III a (Project Ref 162/025/247) and EPSRC CASE for New Academics award GR/P02745/01 for partial financial support of the work described in this paper. The authors thank the EPSRC Engineering Instrument Loan Pool for supplying the high-speed video camera. The contribution of Professor A. Shraiber, Energy Institute, Kiev, Ukraine is gratefully acknowledged.

References

Arai M, Tabata M, Hiroyasu H, Shimizu M (1984) Disintegration Processes and Spray Characterization of Fuel Jet Injected by a Diesel Nozzle. SAE 840275.

Baniasad M S (1994) Analysis of the fuel injection rate in Diesel injection systems. PhD thesis, London University.

Chehroudi B, Chen S H, Bracco F, Onuma Y (1985) On the intact core of full-cone spray. SAE 850126.

Crua C (2002) Combustion Processes in a Diesel Engine. PhD thesis, University of Brighton. www.crua.net/thesis

Dent J C (1971) A Basis For the Comparison of Various Experimental Methods for Studying Spray Penetration. SAE 710571.

Douglas, J F, Gasiorek J M, Swaffield J A (1995) Fluid Mechanics. Longman, London.

Hattori H, Narumiya K, Tsue M, Kadota T (2002) Photographical analysis of Initial Breakup Processes of Diesel spray. Thisel 2002, Conference on Thermal- and fluid Dynamic Process in Diesel Engines.

Heimgartner C, Leipertz A (2000) Investigation on the Primary Spray Breakup Close to the Nozzle of a Common-Rail High Pressure Diesel Injection system. SAE 2000-01-1799.

Hiroyasu H, Arai M (1990) Structure of Fuel Spray in Diesel Engines. SAE 900475.

Karimi E R (1989) High-speed photography of fuel spray and combustion event in a production Diesel engine and combustion bomb. IMech E; pp 269-281.

Kennaird D A, Crua C, Lacoste J, Heikal M R, Gold M R, Jackson N S (2002) In-Cylinder Penetration and Breakup of Diesel Sprays Using a Common Rail Injection System. SAE 2002-01-1626.

Liu AB, Reitz RD (1993) Mechanism of air-assisted liquid atomisation. Atomization and Sprays, vol 3, pp 55-75.

Lucas, Rate of injection manual; High T/P rate gauge manual; issued 11/9/95.

Mulholland JA, Srivastava RK, Wendt JOL (1988) Influence of droplet spacing on drag coefficient in non-evaporating, mono-disperse streams. AIAA Journal, vol 26, No 10.

Naber D, Siebers D L (1996) Effects of Gas Density and vaporization on Penetration and Dispersion of diesel Sprays. SAE 960034.

Nurick W H (1976) Orifice Cavitation and its Effects on Spray Mixing. Journal of Fluids. Engineering.

Payri F, Desantes J M, Arrègla J (1996) Characterization of D.I. Diesel spray in high density conditions. SAE 960774.

Reitz R D, Diwakar R (1987) Structure of High-Pressure Fuel sprays. SAE 870598.

Sazhin S S, Crua, C, Kennaird, D, Heikal M R (2003) The initial stage of fuel spray penetration. Fuel vol 82, pp 875-885.

Sazhin S S, Feng G, Heikal M R (2001) A model for fuel spray penetration. Fuel vol 80 , pp 2171 – 2180.

Sazhina E M, Sazhin S S, Heikal M R, Babushok V I, Johns R J R (2000) A detailed modelling of the spray ignition process in Diesel engines, Comb Sci and Technology, vol 160, pp 317-344.

Thring M W, Newby M P (1952) Combustion length of enclosed turbulent jet flames. 4th International symposium on combustion, Cambridge, Mass, pp 789-796.

Yule A J, Filipovic I (1991) On the breakup times and Length of Diesel Spray. International journal of Heat and Fluid Flow, vol 13, No 2.